Asia-Pacific Journal of Atmospheric Sciences (2021) 57:839–850
https://doi.org/10.1007/s13143-021-00224-7

Online ISSN 1976-7951
Print ISSN 1976-7633

REVIEW PAPER

# Changes in Dust Activity in Spring over East Asia under a Global Warming Scenario

Qi Zong [1,2,3] · Rui Mao [1,2,3] · Dao-Yi Gong [3] · Chenglai Wu [4] · Bing Pu [5] · Xingya Feng [3] · Yijie Sun [3]

Received: 9 June 2020 / Revised: 18 October 2020 / Accepted: 4 January 2021 / Published online: 20 January 2021


## Abstract

Dust activity not only influences human health through dust storms but also affects climate at local and regional scales through the direct effects of dust aerosols on both solar and longwave radiative heating. In this study, based on dust simulations from seven Coupled Model Intercomparison Project Phase 5 (CMIP5) models, the spatial and temporal changes in dust activity over East Asia under a Representative Concentration Pathway 8.5 global warming scenario were examined for the periods of 2016–2035 (P1), 2046–2065 (P2) and 2080–2099 (P3). The results show that the multimodel ensemble mean (MME) of the CMIP5 models largely captures the spatial distribution of dust emissions and dust optical depth (DOD) over East Asia during 1986–2005 (P0). The MME reproduces the increasing trend in dust emissions and DOD over dust sources in East Asia during P0. Accompanying emission reductions during P1 to P3, the DOD simultaneously decreases, and the evident DOD decline can also be found over downwind areas in eastern China and the Korean Peninsula. Simulations project increases in precipitation and the LAI (leaf area index). Simultaneously, the weakened East Asian trough leads to anomalous southerly winds and lower wind speeds at the surface. All these results indicate unfavorable conditions for dust emissions over the sources regions, resulting in a decreased DOD over East Asia during P1 to P3.

**Keywords** Dust activity · CMIP5 · East Asia · Future projection

## 1 Introduction

Dust activity includes dust emissions in dust sources, dust transport in the middle troposphere from dust sources to downwind areas, and dust deposition over source regions and downwind areas (Marticorena and Bergametti 1995). Dust storms over East Asia originate from the mid-latitude arid and semiarid areas of China and Mongolia. Dust particles are emitted into the lower and middle troposphere by dust storms (Zhang and Zhang 1998), which are transported by the westerlies to downwind areas over eastern China, Mongolia, the Korean Peninsula, Japan, the Pacific Ocean, and North America (Chen et al. 2017; Huang et al. 2008; Mahowald et al. 2009, 2017; Uno et al., 2006; Zhao 2003). Dust particles affect not only human health (Chen et al. 2017) but also regional climate through their direct effects on solar and longwave radiation (Chen et al. 2013; Gautam et al. 2013; Lau et al. 2000) and indirect effects on precipitation through aerosol-cloud-precipitation interactions over Asian arid and semiarid regions (Huang et al. 2014; Mahowald et al. 2017; Yin and Chen 2007). The deposition of iron-bearing dust into the ocean provides nutrients for phytoplankton growth, impacting biological productivity, and the carbon cycle. (Tan et al. 2016).

Many studies have examined the changes in East Asian dust activity in the future. Land degradation and desertification will expand in the near future in drylands over East Asia

Responsibility Editor: Yun Gon Lee

✉ Rui Mao
mr@bnu.edu.cn

[1] MOE, Key Laboratory of Environmental Change and Natural Disaster, Beijing Normal University, Beijing 100875, China

[2] MOE, Engineering Research Center of Desertification and Blown–sand Control, Beijing Normal University, Beijing 100875, China

[3] Academy of Disaster Reduction and Emergency Management, Faculty of Geographic Science, Beijing Normal University, Beijing 100875, China

[4] Institute of Center for Climate and Environment Sciences, Institute of Atmospheric Physics, Chinese Academy of Sciences, Beijing, China

[5] Department of Geography and Atmospheric Science, The University of Kansas, Lawrence, KS, USA

under the warming scenarios of Representative Concentration Pathway (RCP) 4.5 and 8.5, which would lead to an increase in dust sources and more dust activity in the future (Huang et al. 2016). However, the mid-latitude circulation is likely to result in a less dusty future due to less windy weather or more precipitation (Rind 1998; Zhang et al. 2019) because of reducing the poleward temperature gradient at middle latitudes in the warming scenarios. Tegen et al. (2004) projected dust emissions in 2040–2050 and 2070–2080 and found the reduction over eastern Asia by 26% and 19%, respectively. Based on ten models in the Coupled Model Intercomparison Project Phase 5 (CMIP5), annual dust emissions in northeast Asia under four warming scenarios are projected to decrease in the future, particularly in the Taklimakan Desert and Gobi Desert significantly (Kim et al. 2014). In addition to dust emissions, Pu and Ginoux (2018) projected a decline in dust optical depth (DOD) over East Asian dust sources and downwind areas in spring and summer by the end of the twenty-first century using the output of seven CMIP5 models and a regression model. To analyze the controlling surface factors, including 10 m wind, bareness, and precipitation that affect CMIP5 DOD, they examined these factors in the observation and CMIP5 models from 2004 to 2016. They found that these three factors mostly represent variation in DOD in the present day, and the projection of variation in DOD is more consistent with changes in precipitation and 10 m wind than that in bareness by the end of the twenty-first century. We mainly focus on dust activity over East Asia and analyze large-scale circulation, which is critical to understanding dust emission and transport in the region and has not been studied much. Thus, this study focuses on the change in dust activity over East Asia in the future and its causes by using seven CMIP5 models. This paper is organized as follows. The data and methods are described in Section 2. We first evaluated simulated historical dust activity (1986–2005) by using MERRA-2 DOD in Section 3.1. In Section 3.2, changes in the dust activity in the near-term (2016–2035), the mid-term (2046–2065), and the far-term future (2080–2099) will be examined. In Section 3.3, we analyze the causes of future changes in East Asian dust activity, including variations in atmospheric circulation and local surface factors such as wind speed, precipitation flux, and leaf area index (LAI). Finally, a summary and discussion are presented in Section 4.

## 2 Data and Method

The current studies were conducted for spring (March, April, and May) because of the frequency of dust storms in spring over East Asia (Mao et al. 2011, 2019; Qian and Shi 2002). We used the dust simulations of seven CMIP5 models (Table 1) following Pu and Ginoux (2018) to project the future changes in dust activity over East Asia. The detailed information of these models refers to the corresponding papers: CanESM2 (Arora et al. 2011), GFDL-CM3 (Donner et al. 2011), HadGEM2-CC and HadGEM2-ES (Collins et al. 2011), MIROC-ESM, and MIROC-ESM-CHEM (Watanabe et al. 2011) and NorESM1-M (Bentsen et al. 2013). The dust emission projection depends on the dust emission scheme and considers some controlling factors, such as near-surface wind, soil types, soil moisture, and surface vegetation coverage. A brief introduction to these seven models and their dust emission schemes is shown in Table 1 (Croft et al. 2005; Marticorena and Bergametti 1995; Paul Ginoux 2001; Reader et al. 1999; Seland et al. 2008; Takemura et al. 2000). In addition, Wu et al. (2018) have evaluated some of aforementioned models and found that except the HadGEM2-ES and HadGEM2-CC model, the most of models reproduced the spatial distribution and the negative long-term trends in dust emission flux over the major dust sources of East Asia during 1961 to 2005. Regarding the HadGEM2-ES and HadGEM2-CC model, we evaluated their performance in simulating spatial distribution of DOD and temporal changes in DOD from 1986 to 2005 (Table 3). The HadGEM2-ES and HadGEM2-CC simulated high DOD over eastern source during 1986–2005. The DOD trend over eastern source was 0.001 and − 0.003 in the simulations of HadGEM2-CC and HadGEM2-ES model, respectively. The DOD from the HadGEM2-CC was consistent with the increasing trend in

**Table 1** Information of the CMIP5 climate models used in this study

| Model name | Lat. × Lon. | Dust emission scheme | Model reference |
|---|---|---|---|
| CanESM2 | 2.8° ×2.8° | Reader et al. (1999), Croft et al. (2005) | Arora et al. (2011) |
| GFDL-CM3 | 2.0° ×2.5° | Paul Ginoux (2001) | Donner et al. (2011) |
| HadGEM2-CC | 1.2° ×1.8° | Marticorena and Bergametti (1995) | Collins et al. (2011) |
| HadGEM2-ES | 1.2° ×1.8° | Marticorena and Bergametti (1995) | Collins et al. (2011) |
| MIROC-ESM | 2.8° ×2.8° | Takemura et al. (2000) | Watanabe et al. (2011) |
| MIROC-ESM-CHEM | 2.8° ×2.8° | Takemura et al. (2000) | Watanabe et al. (2011) |
| NorESM1-M | 1.9° ×2.5° | Seland et al. (2008) | Bentsen et al. (2013) |

DOD over the eastern source derived from the MERRA-2 Reanalysis dataset.

In this study, we examined the simulated dust emission and DOD of the seven models. The CMIP5 models do not provide DOD directly. The formula (Ginoux et al. 2012) for calculating DOD has been used widely by many works, including Kaufman (2005), Ginoux et al. (2012) and Wu et al. (2019). Thus, we converted the dust load to DOD following the formula of Ginoux et al. (2012) for all models as a default method.

$$M = \frac{4\rho r_{eff}}{3Q_{ext}}\tau = \frac{1}{\varepsilon}\tau \quad (1)$$

Equation (1) expressed the relation of DOD ($\tau$) and mass burden M, where $r_{eff}$ = 1.2 μm is the effective radius, $\rho = 2.6 \times 10^6\ g{\cdot}m^{-3}$ is the density of dust, $Q_{ext}$ = 2.5 is the extinction efficiency at 550 nm and for a 1.2 μm particle radius, $\varepsilon = 0.6m^2 \cdot g^{-1}$ is the mass extinction efficiency, and $\tau$ is dust optical depth at 550 nm. In this formula, the effective radius is defined as a constant (1.2 $\mu m$). However, the effective radius range over East Asia is relatively broad (0.01 ~ 100.0 $\mu m$) (Shao and Dong 2006). It is a simplification to apply the same particle radius to the output of all CMIP5 models without considering the discrepancy of radiation effect of dust, which may deteriorate the accuracy of DOD calculation. A bilinear interpolation method was used to unify the grid points with a resolution of 2° × 2.5° in these models for comparative analysis among models. We used the multimodel ensemble mean (MME) to examine the changes of DOD in the near-term (2016–2035, P1), mid-term (2046–2065, P2), and far-term future (2080–2099, P3). To explain the cause of changes in East Asian dust activity in the future, we examined wind field at 500 hPa, geopotential height at 500 hPa (Z500), wind field at 10 m, precipitation flux, and leaf area index (LAI).

The evaluation of dust simulations is a crucial step for future dust projections. We focused our studies on western dust desert, and some semiarid areas in northern China. To examine the simulated DOD from the CMIP5 models, we used observations from the Modern-Era Retrospective analysis for Research and Applications, Version 2 (MERRA-2) Reanalysis dataset (Gelaro et al. 2017). The MERRA-2 Reanalysis dataset provides monthly dust optical thickness (DOT) land surface variables are well constrained by observations in MERRA-2, although DOD is not directly assimilated with satellite products (Randles et al. 2017). We examined the model skills in reproducing DOD during 1986–2005 by using a Taylor diagram (Taylor 2001). In addition, we used the global Met Office Integrated Data Archive System Land and Marine Surface Station data from 1986 to 2005 (UKMIDAS), available from the British Atmospheric Data Center. The UKMIDAS data was used to obtain the occurrence frequency of different types of dust events in the spring season based on the visibility data at 191 stations (Shao et al. 2013). For a given station, a blowing dust day is defined as a day with a record of ww (weather code) =7 (raised dust or sand with visibility of 1–10 km); a dust storm day is the day with a record of ww =9 or 30–32 (strong winds lift large quantities of dust particles, reducing visibility to between 200 and 1000 m). In this study, we used the days of blowing dust and dust storms to indicate the occurrence of dust emission over East Asia.

## 3 Results

### 3.1 Evaluation of CMIP5 Historical Simulations (1986–2005)

Figure 1 shows the spatial distribution of mean DOD in spring derived by CMIP5 models and the MERRA-2 Reanalysis dataset in the period of 1986–2005 (P0). Compared with the spatial distribution of high DOD from the MERRA-2, most CMIP5 models capture the spatial distribution of active dust activity over East Asia in the MERRA-2, i.e., high DOD over the Tarim Basin, the center of northern China, and southern Mongolia. The annual mean DOD of MERRA-2 in spring is 0.169 and 0.103 over the Tarim Basin and the eastern sources. Compared with the value of DOD in the MERRA-2 Reanalysis dataset, the simulated DOD over East Asia from the CMIP5 models is underestimated, particularly in the Tarim Basin. The multimodel ensemble mean (MME) of DOD over the Tarim Basin derived from seven CMIP5 models is less than 0.15, and only three models have DOD above 0.11 over the eastern source (CanESM2, HadGEM2-CC, and HadGEM2-ES).

We evaluated performance of seven CMIP5 models in simulating the annual mean DOD in spring over the Tarim Basin and eastern source during the P0 using a Taylor diagram (Fig. 2). Table 2 shows the spatial correlation coefficient, the ratio of the standard deviation, and the bias (%) and RMSE from the comparison of DOD simulated by 7 CMIP5 models and MERRA-2 based on a historical period (1986–2005) over the Tarim Basin and eastern source. These seven models correlate with MERRA-2 above 0.60 for DOD corresponding to the eastern source; however, only half of the models have DOD values over 0.60 for the Tarim Basin. The standard deviation of DOD in the simulations is lower in the Tarim Basin by a ratio of 0.18–0.48 compared to that in the MERRA-2 Reanalysis dataset. In the eastern source, except HadGEM2-CC and HadGEM2-ES, the standard deviation ratio of simulated DOD is similar to that of the MERRA-2 by 0.75–1.38. The root mean square error (RMSE) of DOD between the CMIP5 models and MERRA-2 over the Tarim Basin and the eastern source is between 0.03 and 0.18. In general, the MME shows better performance than that of most of the models. The ratios of the standard deviation in the

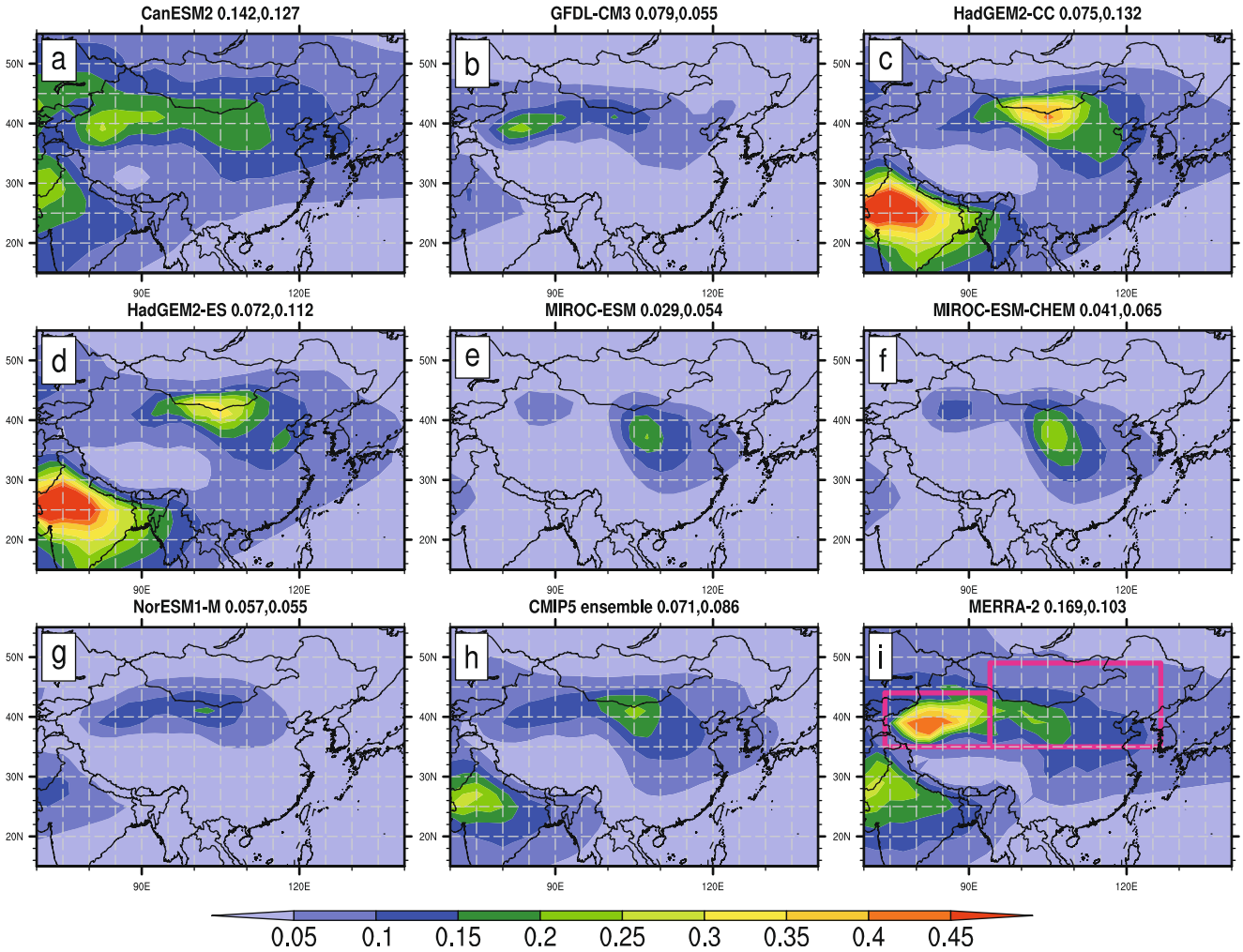


**Fig. 1** **a**–**h** mean dust optical depth (dimensionless quantity) in spring during the historical periods (P0, 1986–2005) from seven CMIP5 models (Table 1) and the multimodel ensemble mean (MME) over the East Asia. The DOD in two study areas is documented in the title of each panel. For comparison, MERRA-2 Reanalysis DOD is showed (**i**). Pink rectangles over the two major sources are marked: western dust source (containing most of Tarim Basin, 33–44°N,74–94°E) and eastern dust source (35–49°N,94–126.5°E, mostly covered the Gobi Desert and other deserts or desertification lands in North China)

**Table 2** Spatial correlation coefficient, the ratio of standard deviation, the bias (%) from the comparison of DOD simulated by 7 CMIP5 models with MERRA-2 based on a historical period (1986–2005) and RMES over Tarim Basin and eastern source

| Model name | Tarim Basin | | | | Eastern source | | | |
|---|---|---|---|---|---|---|---|---|
| | Cor | STD | Bias | RMSE | Cor | STD | Bias | RMSE |
| CanESM2 | 0.84 | 0.48 | −15.80 | 0.08 | 0.88 | 0.82 | 24.03 | 0.03 |
| GFDL-CM3 | 0.93 | 0.46 | −53.25 | 0.11 | 0.88 | 0.75 | −46.49 | 0.05 |
| HadGEM2-CC | 0.44 | 0.31 | −55.61 | 0.14 | 0.69 | 2.20 | 28.39 | 0.07 |
| HadGEM2-ES | 0.39 | 0.27 | −57.23 | 0.14 | 0.69 | 1.77 | 8.80 | 0.05 |
| MIROC-ESM | 0.47 | 0.27 | −75.59 | 0.16 | 0.77 | 1.38 | −36.12 | 0.05 |
| MIROC-ESM-CHEM | 0.41 | 0.18 | −82.84 | 0.18 | 0.69 | 1.17 | −46.94 | 0.06 |
| NorESM1-M | 0.72 | 0.28 | −66.00 | 0.15 | 0.81 | 0.83 | −45.88 | 0.05 |
| MME | 0.76 | 0.28 | −58.05 | 0.14 | 0.83 | 1.14 | −16.30 | 0.03 |

The results of these comparison are shown in Fig. 2

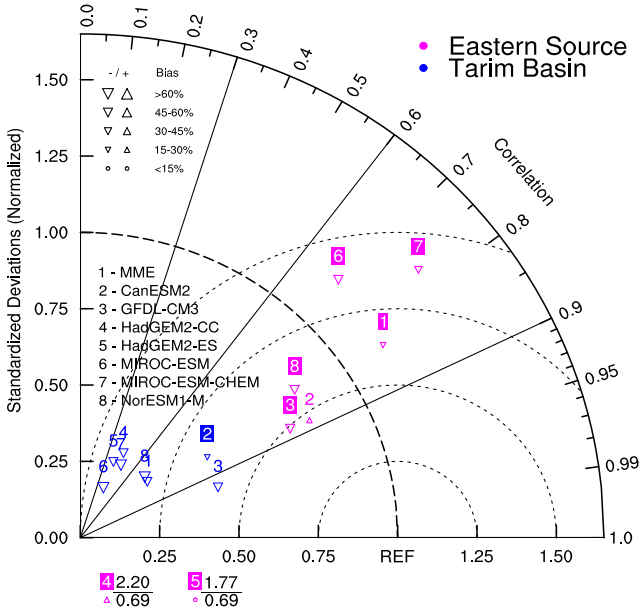


**Fig. 2** Taylor diagram for DOD over Tarim Basin (blue markers) and eastern source (pink markers) among CMIP5 models (seven models and MME) compared with the MERRA-2 Reanalysis data. REF: MEERA-2; azimuthal position: spatial correlation coefficient; radial distance: the ratio of standard deviation; distance from REF point: root mean square error; different symbol with rank size and positive and negative direction: percent bias (%), the minimum bias of the same models filled with background color; further, it plots standard deviations >1.65 as text at the bottom of the figure

MME are 0.14 and 0.03 for the Tarim Basin and eastern source, respectively.

Figure 3 shows the spatial distributions of annual mean dust emission flux in spring over East Asia by the CMIP5 models. For comparison with high-value areas of dust emissions from the CMIP5 models, the spatial distribution of annual mean dust frequency in spring from UKMIDAS is shown (Fig. 3i). The UKMIDAS presents high-frequency regions of dust events over southern Mongolia, the western part of Inner Mongolia, and the Taklimakan Desert. Five out of seven models capture the high dust emission areas in the observations. Except for HadGEM2-CC and HadGEM2-ES, five models show a spatial pattern of dust emission in northern China and southern Mongolia, consistent with high dust frequency from the UKMIDAS. These five models determine the MME of dust emissions, showing two dust emission centers and dust emissions higher in the Gobi Desert than those in the Taklimakan Desert.

Finally, we compared the temporal variations in the simulated DOD and dust emissions during P0 over the Tarim Basin and eastern source (Table 3) with the MERRA-2 Reanalysis dataset and dusty occurrence from UK MIDAS. The MERRA-2 Reanalysis dataset shows an increasing DOD trend in the Tarim Basin (0.011 decade$^{-1}$) and the eastern source (0.014 decade$^{-1}$) during 1986–2005 (P0). However, the MME shows a negative DOD tendency in the Tarim Basin, because only two models (CanESM2 and MIROC-ESM) reproduce the increasing DOD in the Tarim Basin during P0 by 0.001–0.004 per decade. Five models and the MERRA-2 Reanalysis dataset show the increasing trend in DOD over the eastern source; the trend is 0.002, 0.001, 0.011, 0.009, and 0.0004 per decade in CanESM2, GFDL-CM3, HadGEM2-CC, MIROC-ESM-CHEM, and NorESM1-M, respectively. In addition to DOD, the observed trend of dust frequency is −0.65 days per decade for the Taklimakan Desert and 0.52 days per decade for the eastern source. The trends of dust emissions simulated by the MME are consistent with those of dust frequency in both study regions. Three models (GFDL-CM3, HadGEM2-ES, and MIROC-ESM-CHEM) show decreasing dust emissions in the Taklimakan Desert by 0.10–0.21 Tg per decade. Except for MIROC-ESM and NorESM1-M, five models show positive trends in dust emissions in the eastern source. Nearly all models show better performance in the trends of dust emissions and DOD over the eastern source than that over the Taklimakan Desert during P0.

In summary, the MME of the seven CMIP5 models largely captures the spatial distribution of climatological DOD and dust emissions over East Asia with high values over the eastern source and the Tarim Basin. The MME reproduces the increasing trend in DOD and dust emissions over the eastern source and the decreasing dust emissions over the Tarim Basin. Thus, we will use the MME of simulations under the scenario RCP8.5 to project variations in dust activity over East Asia in 2016–2099 under a high warming scenario.

### 3.2 Projection on the Changes in Future Dust Activity (2016–2099)

Figure 4 shows the spatial pattern of changes in dust emissions over East Asia in the future (P1, 2016–2035; P2, 2046–2065; P3, 2080–2099). Compared with that in the historical period (P0, 1986–2005), the MME projects less dust emission over primary dust sources such as the Tarim Basin (−2.68 Tg·yr$^{-1}$) and eastern source (−12.81 Tg·yr$^{-1}$) during P1. Six of the seven models projected negative changes in dust emissions during P1, by 0.35 to 13.16 Tg·yr$^{-1}$ in the Tarim Basin. In the eastern source, two models (HadGEM2-ES, MIROC-ESM-CHEM) dominate the MME of dust emission changes in P1, with a substantial decrease in dust emission over the boundary between Mongolia and China and northern China. Regarding the other five models, there are slight changes in dust emissions in three models (CanESM2, GFDL-CM3, NorESM1-M); HadGEM2-CC (MIROC-ESM) presents increased dust emissions over the boundary between China and Mongolia and decreases the dust emissions over northern China and northeastern China (over central northern China). In the NorESM1-M models, dust emission are unchanged (Kirkevåg et al. 2013; Seland et al. 2008). In P2, the MME

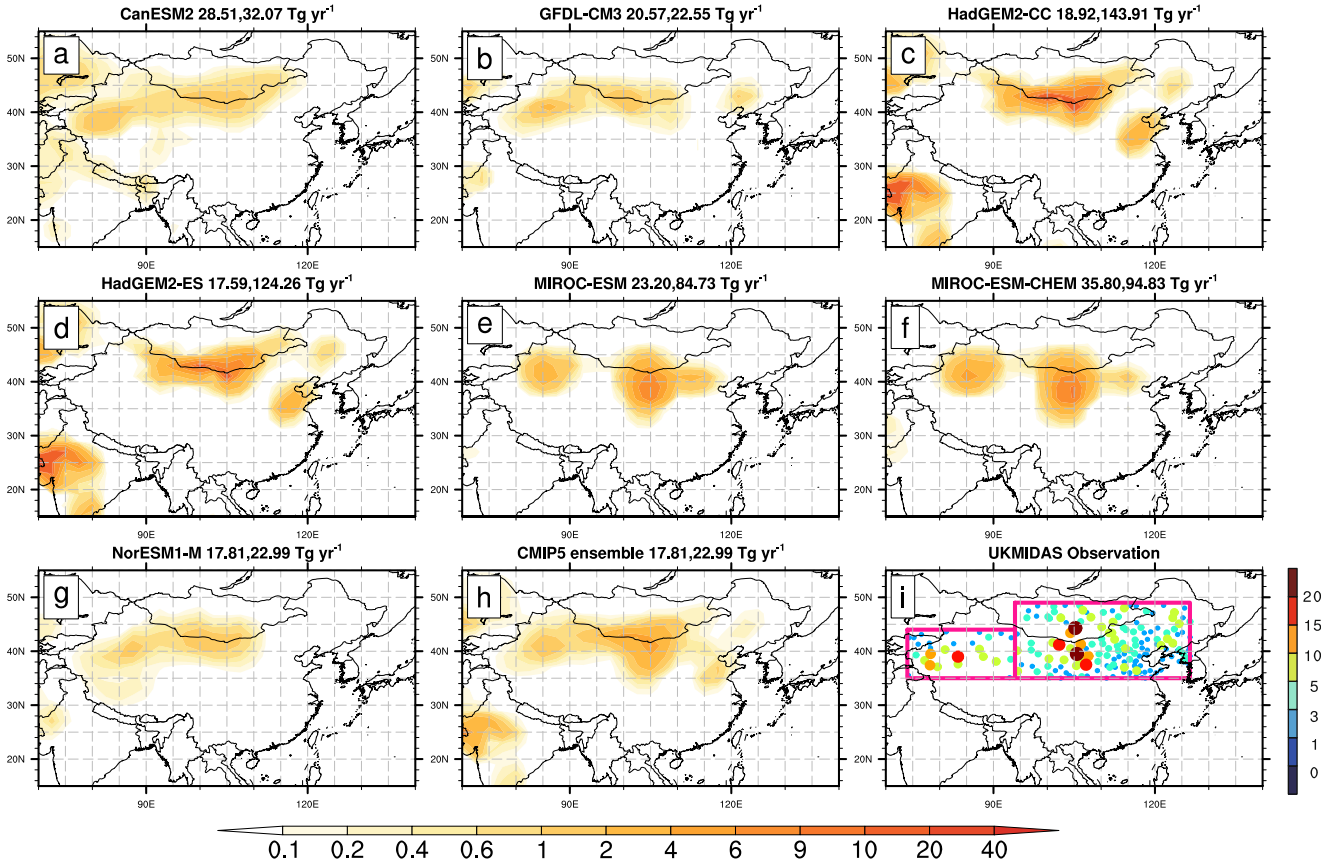


**Fig. 3** **a**–**h** Mean dust emission flux ($Tg\ yr^{-1}$) in spring during the historical period (P0, 1986–2005) from 7 CMIP5 models and MME over the East Asia. The regional dust emission of Tarim Basin and eastern source are documented in the title of each panel. For comparison, dots in (**i**) denote the number of dusty days in spring recorded by UKMIDAS 191 stations averaged during the 1986–2005

(Fig. 4i) projects a more significant decrease in dust emissions than that in P1. However, the spatial distribution of the projected dust emissions in P2 and P3 resembles that in P1.

**Table 3** The modeled linear trends of Tarim Basin and Eastern source for the DOD (unit: per decade) and Dust Emission (unit: Tg per decade), comparing with MERRA-2 Reanalysis DOD and the dusty concurrence of UKMIDAS for the period of 1986 to 2005

| Model name | Tarim Basin | | Eastern source | |
|---|---|---|---|---|
| | DOD | Dust emission | DOD | Dust emission |
| MME | −0.002 | −0.01 | 0.002 | 0.87 |
| CanESM2 | 0.001 | 0.10 | 0.002 | 0.02 |
| GFDL-CM3 | −0.002 | −0.10 | 0.001 | 0.11 |
| HadGEM2-CC | −0.001 | 0.16 | 0.011 | 2.41 |
| HadGEM2-ES | −0.007 | −0.21 | −0.003 | 0.95 |
| MIROC-ESM | 0.004 | 1.79 | −0.007 | −4.39* |
| MIROC-ESM-CHEM | −0.008 | −1.80 | 0.009 | 7.02** |
| NorESM1-M | −0.001 | −0.00 | 0.000 | −0.00 |
| MERRA-2 | 0.011 | – | 0.014 | – |
| UKMIDAS | – | −0.65 | – | 0.52 |

Significance levels from t-test: * $P < 0.01$; ** $P < 0.10$

Most of the models show significantly adverse changes in dust emissions over the Tarim Basin, the boundary between Mongolia and China, northern China, and northeastern China.

Figure 5 shows the changes in DOD over East Asia during P1 to P3. The MME projects a decrease in DOD over northern China in the future (Fig. 5a, i), consistent with previous studies (Pu and Ginoux 2018). Furthermore, we found a DOD decrease over the southeastern part of Mongolia and the Korean Peninsula affected by the weakening emission in the eastern source. In P1, the MME shows negative changes in DOD over the Tarim Basin, central northern China, southeastern China, and the Korean Peninsula compared with that in P0. Six models project a decrease in DOD in the Tarim Basin by −0.009. Three models (HadGEM2-ES, MIROC-ESM, MIROC-EMS-CHEM) show large areas of negative changes by 0.007–0.032 over eastern Asia, southern Korea, and Japan. The projected changes in DOD during P2 and P3 show a similar spatial pattern as that during P1. The MME in P2 (P3) shows negative changes of 0.001 and 0.016 (0.007 and 0.018) over the Tarim Basin and a large area of the negative anomaly over eastern China less than 0.010. Compared to that in P1, DOD decreases more in the MME in P2 and P3 over the Tarim Basin and the eastern source, particularly central northern China.

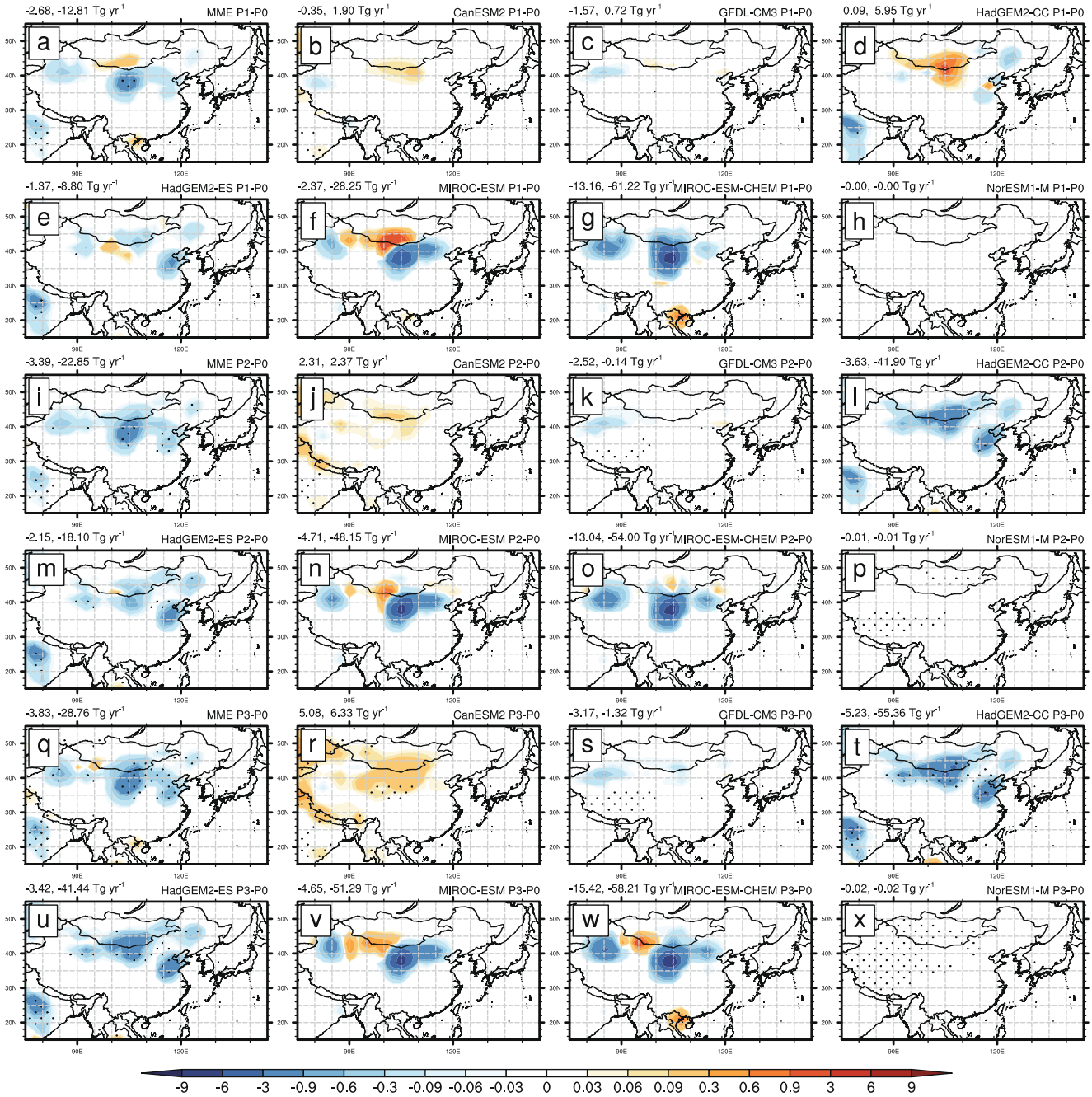


**Fig. 4** **a**–**x** CMIP5 models (7 models and MME) project annual change of dust emission flux in spring for the near-term (P1: 2016–2035), the mid-term (P2: 2046–2065), and the far-term (P3: 2080–2099) compared with the historical period (P0: 1986–2005) over East Asia. The dotted area means the region where dust emission flux in the P1, P2, P3 and reference periods(P0) area are significantly differently ($p < 0.05$ in t-test)

### 3.3 Analysis of the Mechanism of Changing Dust Activity in the Future

We first discussed the causes of dust emissions changes by considering wind speed at 10 m above the ground, precipitation flux, and leaf area index (LAI) (Fig. 6). Compared to those in the historical period (P0, 1986–2005), the change percentage of precipitation and LAI gradually increase from P1 to P3 in the Tarim Basin. The precipitation and LAI increase by 4–45% and 4–72% in P1, by 15–52% and 25–225% in P2, and by 15–66% and 16–75% in P3, respectively. Regarding surface wind speed, except for the GFDL-CM3 and MIROC-ESM models, most models show decreased wind speed at 10 m above the ground from P1 to P3. The MME values of surface wind speed, precipitation, and LAI are −11.9%, 12.0%, and 18.7% during the P1, −20.5%, 21.4%,

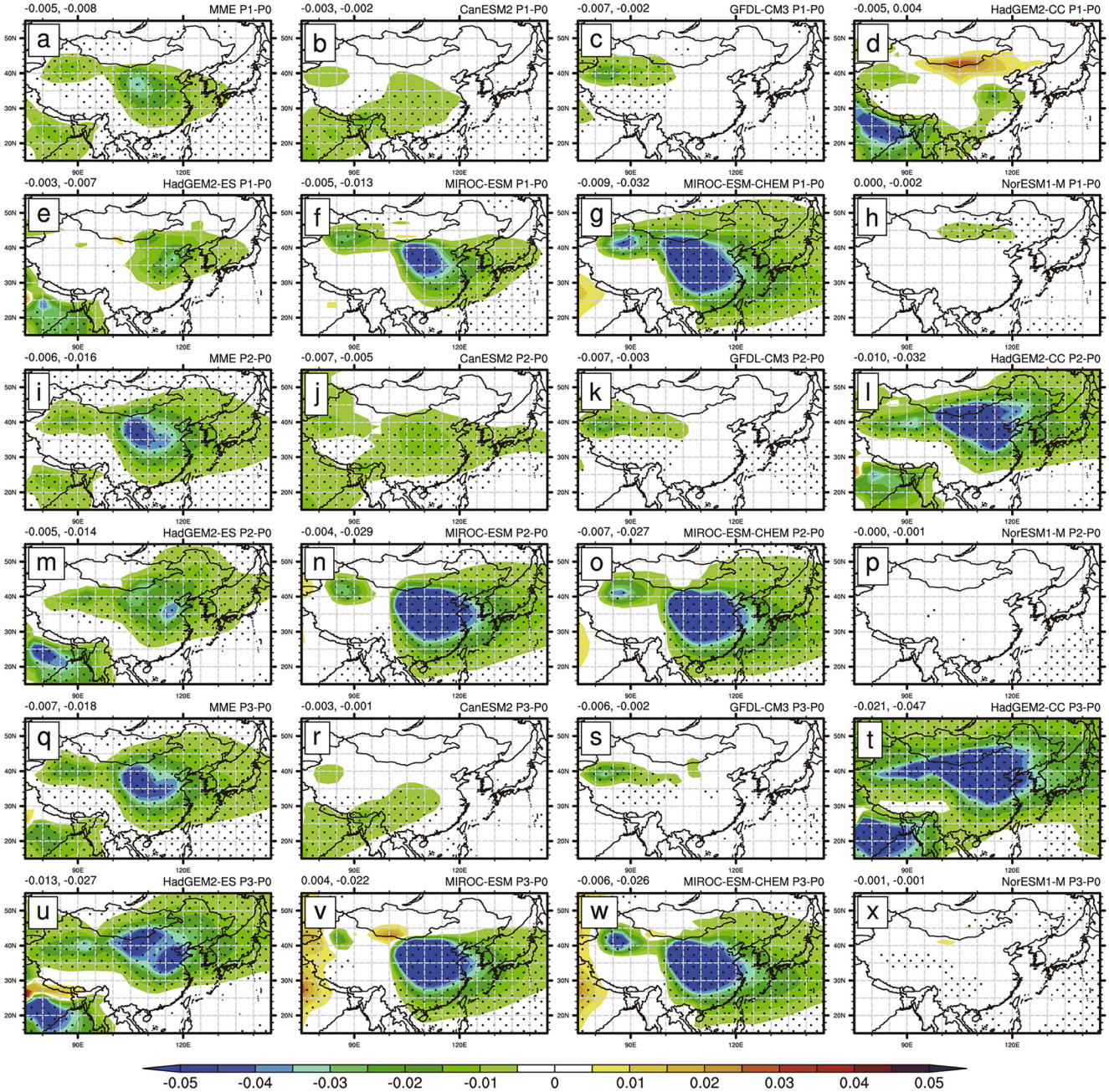


**Fig. 5** **a**–**x** CMIP5 models (7 models and MME) project annual change of DOD in spring for the near-term (P1: 2016–2035), the mid-term (P2: 2046–2065), and far-term (P3: 2080–2099) compared with the historical period (1986–2005) over East Asia. The dotted area is the same as Fig. 4 ($p < 0.05$ in t-test)

63.0% during the P2, and − 30.5%, 26.0%, 50.244% during the P3, respectively. Therefore, a massive increase in precipitation and LAI during P1 to P3, and a decrease in surface wind speed, play a role in less dust emission. In addition, compared to those in P0, precipitation and LAI primarily increase in the eastern source by 6.8–48.6% (15.4–66.1%, 23–60%) and 1.1–43.5% (17.0–76.0%, 34%–124%) in the models in P1 (P2, P3). Except for three models, nearly all models show slightly decreased wind speeds at 10 m above the ground in P1 to P3 compared with that in P0. As a result, the MME values of surface wind speed, precipitation, and LAI are −12.4% (−13.9%, −37.2%), 11.4% (26.0%, 38.4%), and 18.0% (51.0%, 95.6%) during P1 (P2, P3), respectively. An increase in the precipitation and LAI and a decrease in surface wind speed during P1 to P3 play a role in the decrease in dust emissions over the eastern source compared with that in P0 (Fig. 6).

The decrease in DOD over East Asia in P1 to P3 is caused by less dust emission over the Tarim Basin and eastern source. Besides, atmospheric circulation changes in the lower to

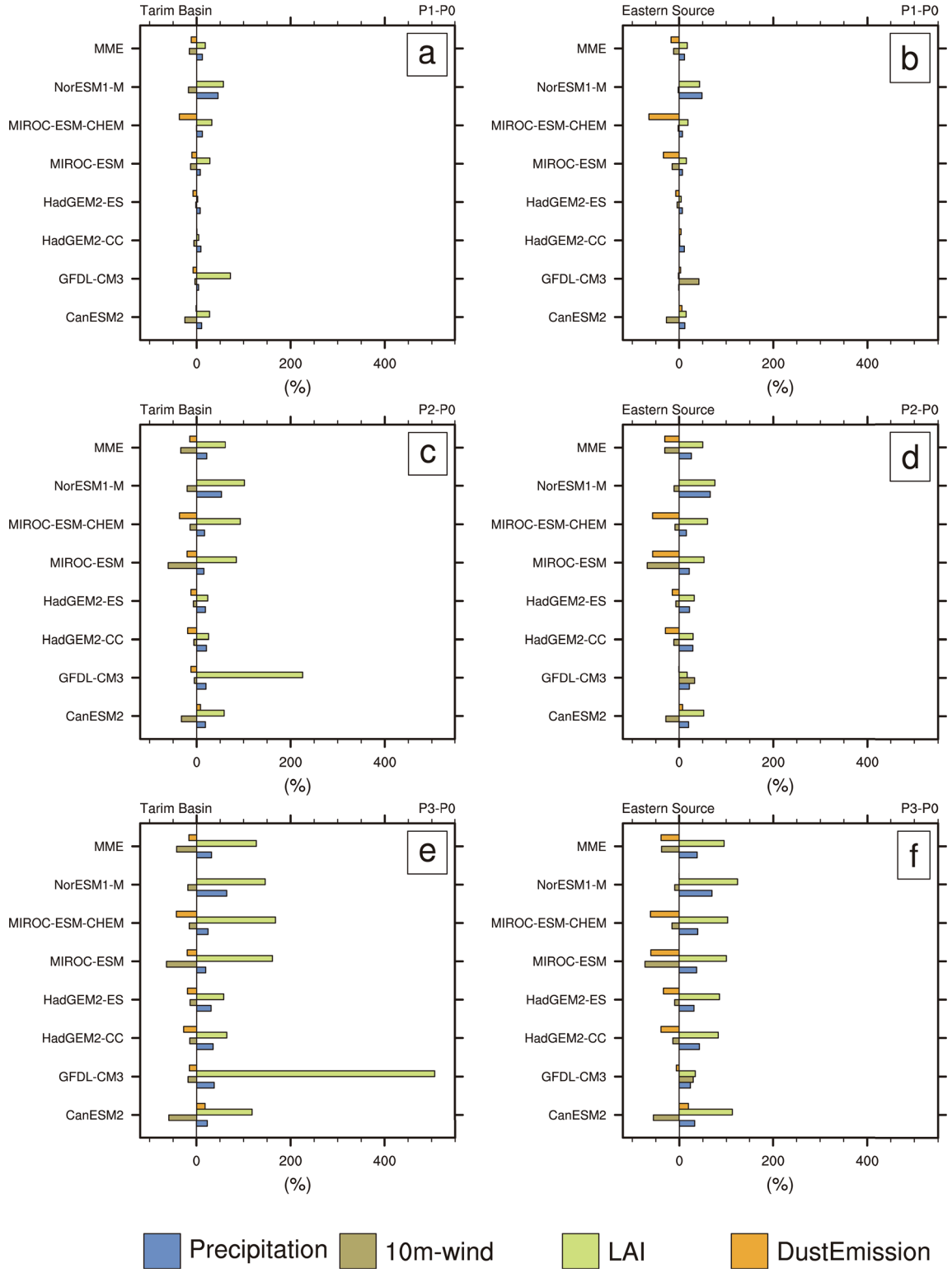


**Fig. 6** **a**–**f** Bar plot showing the change in percentage change for the near-term (P1:2016–2035), the mid-term (P2: 2046–2065), and the far-term (P3: 2080–2099) compared with the reference period (P0: 1986–2005). The legend shows the dust emission and surface controlling factors precipitation flux, 10-m wind, leaf area index (LAI)

middle troposphere may be critical determinants for decreasing DOD in the downwind regions. Figure 7 shows the changes simulated by the MME in the wind field at 500 hPa (Z500) and the wind at the surface in spring. The corresponding historical data are examined in Figs. S1 and S2. As shown in the figure, a significant decrease in surface wind speed is

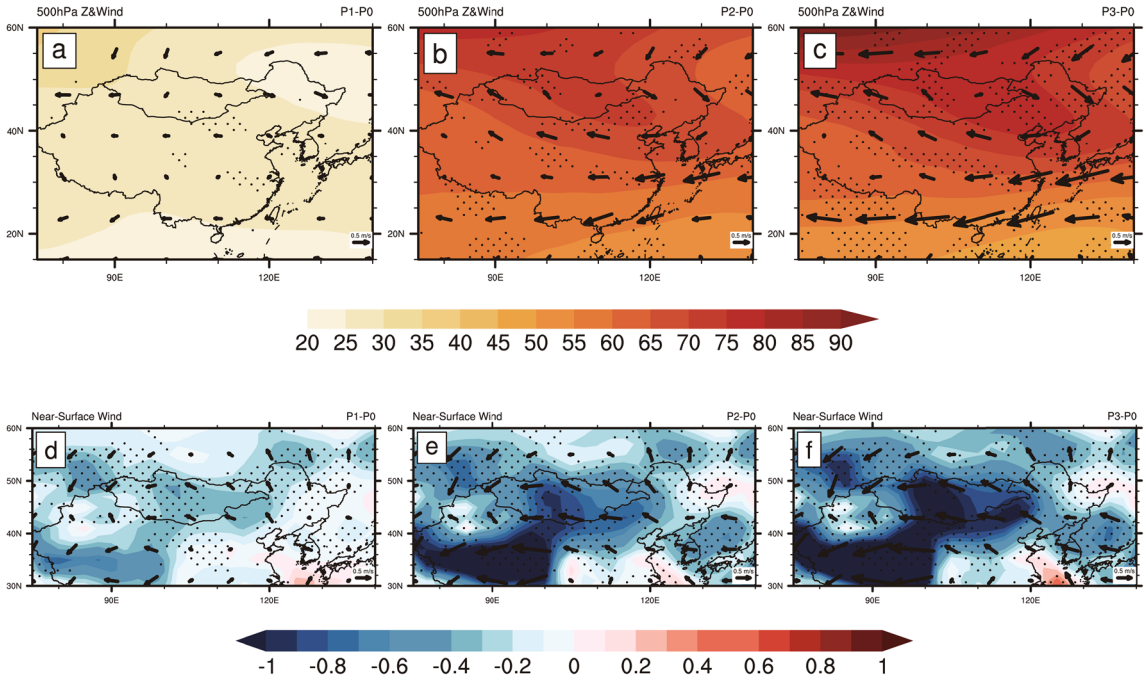


**Fig. 7** **a–f** Multi-model simulations for the annual change of geopotential height, wind field at 500hPa and 10m wind above the groundin spring for (P1: 2016–2035), the mid-term (P2, 2046–2065), and the far-term (P3: 2080–2099) compared with the reference period(P0: 1986–2005). The dotted area is the same as Fig. 4 ($p < 0.05$ in t-test)

presented over the Tarim Basin and eastern source during P1 to P3 (Fig. 7). Weakly wind anomalies and decreased northwesterly winds at the surface enhance the decrease in dust emissions from the eastern sources in three studied periods. The Z500 anomalies show weak positive height anomalies in P1 and gradually strong positive height anomalies in P2 to P3 with a center across Mongolia. The height anomalies induce weak winds in East Asia and southeasterly wind anomalies over Mongolia and northern China at the 500 hPa level during P1 to P3. The weak winds in P1 and decreased northwesterly winds in P2 and P3 are not favorable for the transport of dust from the source to downwind regions in East Asia, resulting in a decreased DOD over East Asia.

## 4 Summary and Discussion

This study used seven CMIP5 models (CanESM2, GDFL-CM3, HadGEM2-ES, HadGEM2-CC, MIROC-ESM, MIROC-ESM-CHEM, NorESM1-M) to project dust activity in the future. We first evaluated the modelling skills of these seven models in simulating East Asian dust activity by comparing it with MERRA-2 Reanalysis dataset and UKMIDAS. We found that the MME of the CMIP5 models can largely reproduce the spatial distribution of climatological DOD and dust emissions over East Asia with a high value over the eastern source and Tarim Basin during 1986–2005 (P0). The MME reproduces increasing trends in dust emissions and DOD over the eastern source and a decreasing trend in dust emissions over the Tarim Basin in the 1986–2005 period. Based on the simulations of these seven models under the RCP8.5 warming scenario, dust activity variability over East Asia in the near-term future (2016–2035, P1), the mid-term (2046–2065, P2) and the far-term (2080–2099, P3) were examined. Compared to that in P0, the MME projects a decrease in dust emissions by 2.68 and 12.81 (3.39 and 22.85, 3.83 and 28.76) $Tg{\cdot}yr^{-1}$ over the Tarim Basin and eastern source in the near-term (the mid-term, the far-term), respectively. Meanwhile, a large area of the negative anomaly of DOD is shown over eastern China, the Korea Peninsula, the Far East, and Japan with a center over eastern China in P1 to P3 relative to that in P0.

The decrease in dust emissions over the Tarim Basin and the eastern source is mainly caused by local surface controlling factors, such as a decrease in surface wind speed (−37 ~ −11%) and an increase in precipitation (+11 ~ 38%) and LAI (+18 ~ 95%) in three studied periods. The decrease in DOD over East Asia from P1 to P3 is related to less dust emission over the Tarim Basin and eastern source. Besides, changes in atmospheric circulation in the lower to middle troposphere may be key determinants for decreasing DOD in the downwind regions. There is a weakened East Asian trough in the middle troposphere during P1 to P3, compared to that in P0. Therefore, the decrease in northwesterly winds in the middle troposphere prohibits dust transport to the Korean Peninsula and southeastern China.

It is worth noting that there are difference in the DOD simulations over the Tarim Basin among the seven models.

Moreover, the simulated DOD of models show low values over the Tarim Basin than the eastern source which is opposite to that derived by the MERRA-2 Reanalysis dataset. To reduce this inaccuracy of simulations over the Tarim Basin, we have only analyzed models (CanESM2, GFDL-CM3) that have good performance in simulating the higher DOD over the Tarim Basin than the eastern sources. The CaneESM2 and GFDL-CM3 show a reduction of dust emission in the Tarim Basin during P1 to P3 compared to P0 (Fig. S3). Figure S4 showed a large area of decreased DOD over the Tarim Basin during P1 and P3, and over the northern China during P2 as to compared with that in P0. The corrected result is consistent with the decreased dust emission over the Tarim Basin and decreased DOD in East Asia derived from the ensemble mean of aforementioned seven models.

Moreover, it should be mentioned that the local thermal conditions in Tarim Basin can cause the dust devil (Han et al. 2016; Tang et al. 2018), which affecting dust emission. This process had not been considered in the dust emission schemes of CMIP5 models (e.g., Marticorena and Bergametti 1995, Takemura et al. 2000), which maybe a reason for the lower DOD over the Tarim Basin in the simulations as to compare with that over the eastern source. The issue will be studied in the further work.

**Supplementary Information** The online version contains supplementary material available at https://doi.org/10.1007/s13143-021-00224-7.

**Acknowledgements** We thank Prof. Yaping Shao and Dr. Martina Klose for analyzing the dust observations from the global Met Office Integrated Data Archive System, UK Meteorological Office. This research was supported by the National Key R&D Program of China (2016YFA0602401). Mao was supported by the National Natural Science Foundation of China (41571039, 41730639). Q. Zong is supported by the Key Laboratory of Environmental Change and Natural Disaster and Engineering Research Center of Desertification and Blownsand Control. We would like to thank the high-performance computing support from the Center for Geodata and Analysis, Faculty of Geographical Science, Beijing Normal University [https://gda.bnu.edu.cn/].

CMIP5 data is downloaded from https://esgf-node.llnl.gov/search/cmip5/ (last access February 2020).MERRA-2 Reanalysis data is download from https://disc.gsfc.nasa.gov/daac-bin/FTPSubset2.pl?LOOKUPID_List=M2I3NVAER (last access February 2019). Met Office Integrated Data Archive System (MIDAS) Land and Marine Surface Stations Data (1853-current) is downloaded from http://catalogue.ceda.ac.uk/uuid/220a65615218d5c9cc9e4785a3234bd0 (last access February 2020).

## References

Arora, V.K., Scinocca, J.F., Boer, G.J., Christian, J.R., Denman, K.L., Flato, G.M., Kharin, V.V., Lee, W.G., Merryfield, W.J.: Carbon emission limits required to satisfy future representative concentration pathways of greenhouse gases. Geophys. Res. Lett. **38**(5), (2011). https://doi.org/10.1029/2010gl046270

Bentsen, M., Bethke, I., Debernard, J.B., Iversen, T., Kirkevåg, A., Seland, D.H., Roelandt, C., Seierstad, I.A., Hoose, C., Kristjánsson, J.E.: The norwegian earth system model, noresm1-m part 1: description and basic evaluation of the physical climate. Geosci. Model Dev. **6**(3), 687–720 (2013). https://doi.org/10.5194/gmd-6-687-2013

Chen, S., Huang, J., Zhao, C., Qian, Y., Leung, L.R., Yang, B.: Modeling the transport and radiative forcing of taklimakan dust over the tibetan plateau: a case study in the summer of 2006. J. Geophys. Res. Atmos. **118**(2), 797–812 (2013). https://doi.org/10.1002/jgrd.50122

Chen, S., Huang, J., Qian, Y., Zhao, C., Kang, L., Yang, B., Wang, Y., Liu, Y., Yuan, T., Wang, T., Ma, X., Zhang, G.: An overview of mineral dust modeling over east asia. J. Meteorol. Res. **31**(4), 633–653 (2017). https://doi.org/10.1007/s13351-017-6142-2

Ginoux, P., Chin, M., Tegen, I., Prospero, J.M., Holben, B., Dubovik, O., Lin, S.-J.: Sources and distributions of dust aerosols simulated with the GOCART model. J. Geophys. Res: Atmos. **106**(D17), 20255–20273 (2001). https://doi.org/10.1029/2000jd000053

Collins, W.J., Bellouin, N., Doutriaux-Boucher, M., Gedney, N., Halloran, P., Hinton, T., Hughes, J., Jones, C.D., Joshi, M., Liddicoat, S., Martin, G., O'Connor, F., Rae, J., Senior, C., Sitch, S., Totterdell, I., Wiltshire, A., Woodward, S.: Development and evaluation of an Earth-System model – HadGEM2. Geosci. Model Dev. **4**(4), 1051–1075 (2011). https://doi.org/10.5194/gmd-4-1051-2011

Croft, B., Lohmann, U., von Salzen, K.: Black carbon ageing in the Canadian Centre for Climate modelling and analysis atmospheric general circulation model. Atmos. Chem. Phys. **5**(7), 1931–1949 (2005). https://doi.org/10.5194/acp-5-1931-2005

Donner, L.J., Wyman, B.L., Hemler, R.S., Horowitz, L.W., Ming, Y., Zhao, M., Golaz, J.C., Ginoux, P., Lin, S.J., Schwarzkopf, M.D., Austin, J., Alaka, G., Cooke, W.F., Delworth, T.L., Freidenreich, S.M., Gordon, C.T., Griffies, S.M., Held, I.M., Hurlin, W.J., Klein, S.A., Knutson, T.R., Langenhorst, A.R., Lee, H.C., Lin, Y., Magi, B.I., Malyshev, S.L., Milly, P.C.D., Naik, V., Nath, M.J., Pincus, R., Ploshay, J.J., Ramaswamy, V., Seman, C.J., Shevliakova, E., Sirutis, J.J., Stern, W.F., Stouffer, R.J., Wilson, R.J., Winton, M., Wittenberg, A.T., Zeng, F.: The dynamical core, physical parameterizations, and basic simulation characteristics of the atmospheric component am3 of the gfdl global coupled model cm3. J. Clim. **24**(13), 3484–3519 (2011). https://doi.org/10.1175/2011jcli3955.1

Gautam, R., Hsu, N.C., Lau, W.K.M., Yasunari, T.J.: Satellite observations of desert dust-induced himalayan snow darkening. Geophys. Res. Lett. **40**(5), 988–993 (2013). https://doi.org/10.1002/grl.50226

Gelaro, R., McCarty, W., Suarez, M.J., Todling, R., Molod, A., Takacs, L., Randles, C., Darmenov, A., Bosilovich, M.G., Reichle, R., Wargan, K., Coy, L., Cullather, R., Draper, C., Akella, S., Buchard, V., Conaty, A., da Silva, A., Gu, W., Kim, G.K., Koster, R., Lucchesi, R., Merkova, D., Nielsen, J.E., Partyka, G., Pawson, S., Putman, W., Rienecker, M., Schubert, S.D., Sienkiewicz, M., Zhao, B.: The Modern-Era Retrospective Analysis for Research and Applications, Version 2 (MERRA-2). J. Clim. **30**(13), 5419–5454 (2017). https://doi.org/10.1175/JCLI-D-16-0758.1

Ginoux, P., Clarisse, L., Clerbaux, C., Coheur, P.F., Dubovik, O., Hsu, N.C., Van Damme, M.: Mixing of dust and $nh_3$ observed globally over anthropogenic dust sources. Atmos. Chem. Phys. **12**(16), 7351–7363 (2012). https://doi.org/10.5194/acp-12-7351-2012

Han, Y., Wang, K., Liu, F., Zhao, T., Yin, Y., Duan, J., Luan, Z.: The contribution of dust devils and dusty plumes to the aerosol budget in western China. Atmos. Environ. **126**, 21–27 (2016). https://doi.org/10.1016/j.atmosenv.2015.11.025

Huang, J., Minnis, P., Chen, B., Huang, Z., Liu, Z., Zhao, Q., Yi, Y., Ayers, J.K.: Long-range transport and vertical structure of asian dust from calipso and surface measurements during pacdex. J. Geophys. Res. **113**(D23), (2008). https://doi.org/10.1029/2008jd010620

Huang, J., Wang, T., Wang, W., Li, Z., Yan, H.: Climate effects of dust aerosols over east asian arid and semiarid regions. J. Geophys. Res. Atmos. **119**(19), 11,398–11,416 (2014). https://doi.org/10.1002/2014jd021796

Huang, J., Yu, H., Guan, X., Wang, G., Guo, R.: Accelerated dryland expansion under climateăchange. Nat. Clim. Chang. **6**(2), 166–171 (2016). https://doi.org/10.1038/nclimate2837

Kaufman, Y.J.: Dust transport and deposition observed from the terra-moderate resolution imaging spec-troradiometer (modis) spacecraft over the Atlantic Ocean. J. Geophys. Res. **110**(D10), (2005). https://doi.org/10.1029/2003jd004436

Kim, T., Boo, K.O., Lee, J., Cho, C.: Analysis of the future emission changes in mineral dust aerosol in cmip5 related to bare soil and soil moisture conditions. J. Clim. Res. **9**(1), 33–51 (2014). https://doi.org/10.14383/cri.2014.9.1.33

Kirkevåg, A., Iversen, T., Seland, H.C., Kristjánsson, J.E., Struthers, H., Ekman, A.M.L., Ghan, S., Griesfeller, J., Nilsson, E.D., Schulz, M.: Aerosolclimate interactions in the norwegian earth system model noresm1-m. Geosci. Model Dev. **6**(1), 207–244 (2013). https://doi.org/10.5194/gmd-6-207-2013

Lau, K.M., Kim, K.M., Yang, S.: Dynamical and Boundary Forcing Characteristics of Regional Components of the Asian Summer Monsoon. J. Clim. **13**(14), 2461–2482 (2000). https://doi.org/10.1175/1520-0442(2000)013<2461:DABFCO>2.0.CO;2

Mahowald, N.M., Engelstaedter, S., Luo, C., Sealy, A., Artaxo, P., Benitez-Nelson, C., Bonnet, S., Chen, Y., Chuang, P.Y., Cohen, D.D., Dulac, F., Herut, B., Johansen, A.M., Kubilay, N., Losno, R., Maenhaut, W., Paytan, A., Prospero, J.M., Shank, L.M., Siefert, R.L.: Atmospheric iron deposition: global distribution, variability, and human perturbations. Ann. Rev. Mar. Sci. **1**, 245–278 (2009). https://doi.org/10.1146/annurev.marine.010908.163727 https://www.ncbi.nlm.nih.gov/pubmed/21141037

Mahowald, N.M., Scanza, R., Brahney, J., Goodale, C.L., Hess, P.G., Moore, J.K., Neff, J.: Aerosol deposition impacts on land and ocean carbon cycles. Curr. Clim. Chang. Rep. **3**(1), 16–31 (2017). https://doi.org/10.1007/s40641-017-0056-z

Mao, R., Gong, D., Bao, J., Fan, Y.: Possible influence of arctic oscillation on dust storm frequency in North China. J. Geogr. Sci. **21**(2), 207–218 (2011). https://doi.org/10.1007/s11442-011-0839-4

Mao, R., Hu, Z., Zhao, C., Gong, D.Y., Guo, D., Wu, G.: The source contributions to the dust over the tibetan plateau: a modelling analysis. Atmos. Environ. **214**, 116859 (2019). https://doi.org/10.1016/j.atmosenv.2019.116859

Marticorena, B., Bergametti, G.: Modeling the atmospheric dust cycle 1, design of a soil-derived dust emission scheme. J. Geophys. Res.-Atmos. **100**, 1641516430 (1995)

Pu, B., Ginoux, P.: How reliable are cmip5 models in simulating dust optical depth? Atmos. Chem. Phys. **18**(16), 12491–12510 (2018). https://doi.org/10.5194/acp-18-12491-2018

Qian, L.S.Q.W.-H., Shi, S.Y.: Variations of the dust storm in China and its climatic control. J. Clim. **15**, 1216–1229 (2002)

Randles, C.A., Da Silva, A.M., Buchard, V., Colarco, P.R., Darmenov, A., Govindaraju, R., Smirnov, A., Holben, B., Ferrare, R., Hair, J., Shinozuka, Y., Flynn, C.J.: The merra-2 aerosol reanalysis, 1980 - onward, part i: system description and data assimilation evaluation. J. Clim. **30**(17), 6823–6850 (2017). https://doi.org/10.1175/JCLI-D-16-0609.1 https://www.ncbi.nlm.nih.gov/pubmed/29576684

Reader, M.C., Fung, I., McFarlane, N.: The mineral dust aerosol cycle during the last glacial maximum. J. Geophys. Res. Atmos. **104**(D8), 9381–9398 (1999). https://doi.org/10.1029/1999jd900033

Rind, D.: Latitudinal temperature gradients and climate change. J. Geophys. Res. Atmos. **103**(D6), 5943–5971 (1998). https://doi.org/10.1029/97jd03649

Seland, I.T., KirkevÅG, A.L.F., Storelvmo, T.: Aerosol-climate interactions in the cam-Oslo atmospheric gcm and investigation of associated basic shortcomings. Tellus A. **60**(3), 459–491 (2008). https://doi.org/10.1111/j.1600-0870.2008.00318.x

Shao, Y., Dong, C.H.: A review on east asian dust storm climate, modelling and monitoring. Glob. Planet. Chang. **52**(1–4), 1–22 (2006). https://doi.org/10.1016/j.gloplacha.2006.02.011

Shao, Y., Klose, M., Wyrwoll, K.H.: Recent global dust trend and connections to climate forcing. J. Geophys. Res. Atmos. **118**(19), 11, 107–11,118 (2013). https://doi.org/10.1002/jgrd.50836

Takemura, T., Okamoto, H., Maruyama, Y., Numaguti, A., Higurashi, A., Nakajima, T.: Global three-dimensional simulation of aerosol optical thickness distribution of various origins. J. Geophys. Res. Atmos. **105**(D14), 17853–17873 (2000). https://doi.org/10.1029/2000jd900265

Tan, S., Li, J., Gao, H., Wang, H., Che, H., Chen, B.: Satellite-observed transport of dust to the East China Sea and the north pacific subtropical gyre: contribution of dust to the increase in chlorophyll during spring 2010. Atmosphere. **7**(11), (2016). https://doi.org/10.3390/atmos7110152

Tang, Y., Han, Y., Liu, Z.: Temporal and spatial characteristics of dust devils and their contribution to the aerosol budget in east asiaan analysis using a new parameterization scheme for dust devils. Atmos. Environ. **182**, 225–233 (2018). https://doi.org/10.1016/j.atmosenv.2018.03.050

Taylor, K.E.: Summarizing multiple aspects of model performance in a single diagram. J. Geophys. Res. Atmos. **106**(D7), 7183–7192 (2001). https://doi.org/10.1029/2000jd900719

Tegen, I., Werner, M., Harrison, S.P., Kohfeld, K.E.: Relative importance of climate and land use in determining present and future global soil dust emission. Geophys. Res. Lett. **31**(5), (2004). https://doi.org/10.1029/2003gl019216

Uno, I., Wang, Z., Chiba, M., Chun, Y.S., Gong, S.L., Hara, Y., Jung, E., Lee, S.S., Liu, M., Mikami, M., Music, S., Nickovic, S., Satake, S., Shao, Y., Song, Z., Sugimoto, N., Tanaka, T., Westphal, D.L.: Dust model intercomparison (dmip) study over asia: overview. J. Geophys. Res. **111**(D12), (2006). https://doi.org/10.1029/2005jd006575

Watanabe, S., Hajima, T., Sudo, K., Nagashima, T., Takemura, T., Okajima, H., Nozawa, T., Kawase, H., Abe, M., Yokohata, T., Ise, T., Sato, H., Kato, E., Takata, K., Emori, S., Kawamiya, M.: Miroc-esm 2010: model description and basic results of cmip5-20c3m experiments. Geosci. Model Dev. **4**(4), 845–872 (2011). https://doi.org/10.5194/gmd-4-845-2011

Wu, C., Lin, Z., Liu, X., Li, Y., Lu, Z., Wu, M.: Can climate models reproduce the decadal change of dust aerosol in east asia? Geophys. Res. Lett. **45**(18), 9953–9962 (2018). https://doi.org/10.1029/2018gl079376

Wu, M., Liu, X., Yang, K., Luo, T., Wang, Z., Wu, C., Zhang, K., Yu, H., Darmenov, A.: Modeling dust in east asia by cesm and sources of biases. J Geophys Res Atmos. **124**(14), 8043–8064 (2019). https://doi.org/10.1029/2019JD030799 https://www.ncbi.nlm.nih.gov/pubmed/32637292

Yin, Y., Chen, L.: The effects of heating by transported dust layers on cloud and precipitation: a numerical study. Atmos. Chem. Phys. **7**, 34973505 (2007)

Zhang, X.Y., Arimoto, R., Zhu, G.H., Chen, T., Zhang, G.Y.: Concentration, size-distribution and deposition of mineral aerosol over Chinese desert regions. Tellus B **50**(4), 317–330 (1998). https://doi.org/10.1034/j.1600-0889.1998.t01-3-00001.x

Zhang, L., Hay, W.W., Wang, C., Gu, X.: The evolution of latitudinal temperature gradients from the latest cretaceous through the present. Earth Sci. Rev. **189**, 147–158 (2019). https://doi.org/10.1016/j.earscirev.2019.01.025

Zhao, T.L.: Modeled size-segregated wet and dry deposition budgets of soil dust aerosol during ace-asia 2001: implications for trans-pacific transport. J. Geophys. Res. **108**(D23), (2003). https://doi.org/10.1029/2002jd003363